JOURNAL OF CATALYSIS 145, 479–490 (1994)

Effects of Altervalent Cation Doping of TiO_2 on H_2 and CO Adsorption on Supported Rh

Theophilos Ioannides and Xenophon E. Verykios[1]

Institute of Chemical Engineering and High Temperature Chemical Processes, Department of Chemical Engineering, University of Patras, GR-265 00, Patras, Greece

Received November 9, 1992; revised August 4, 1993

The influence of W^{6+}-doping of TiO_2 carriers on the mode of H_2 and CO adsorption on Rh crystallites dispersed on their surfaces is investigated. It is shown that the electrical conductivity of W^{6+}-doped TiO_2 is enhanced while the activation energy of electron conduction is reduced. The capacity of Rh to adsorb H_2 at equilibrium is found to increase monotonically with increasing W^{6+}-dopant concentration in the carrier, while the strength of the adsorption bond is not significantly affected. The capacity of Rh to adsorb CO goes through a maximum at a W^{6+}-dopant concentration of 0.22 atom% in the TiO_2 matrix. The strength of the CO adsorption bond is weakened when Rh is dispersed on doped TiO_2. These phenomena are attributed to long-range electronic interactions at the metal–support interface which alter the work function of surface metal atoms, as well as to short-range electronic interactions at the gas–metal–support interface. © 1994 Academic Press, Inc.

INTRODUCTION

The effects of altervalent cation doping of TiO_2 carriers on the chemisorptive and catalytic properties of supported Pt catalysts have been discussed in previous publications (1–4). Doping implies incorporation of a foreign cation in the crystal structure of the parent material, either replacing the parent cation or being incorporated interstitially in the crystal matrix. As a result of the doping procedure the electronic structure of the semiconductor is altered. Thus, doping with cations of higher valence increases the *n*-type semiconductivity of TiO_2 or raises its Fermi energy level and lowers its work function (5). The opposite is expected upon doping with lower valence cations.

Altervalent doped TiO_2 was used as a carrier of highly dispersed Pt catalysts (1–4). It was observed that Pt dispersed on higher-valence-doped TiO_2 loses a significant fraction of its capacity to adsorb H_2 and CO at equilibrium while the Pt–C bonds were found to be weakened. The same catalysts were also observed to exhibit reduced activity (turnover frequency) for CO oxidation and, primarily, for CO hydrogenation. These phenomena were found to be sensitive to the average size of the metal (Pt) crystallites, their intensity decreasing with increasing crystallite size. The origin of this phenomenon was attributed to electronic interactions at the metal–support interface which alter electronic parameters of the interface metal atoms (short-range effect) and surface metal atoms (long-range effect). The latter was proposed earlier, primarily by Schwab (6) and by Solymosi *et al.* (7, 8).

In the present study, the influence of altervalent cation doping of TiO_2 on the chemisorptive and kinetic behavior of Rh crystallites dispersed on its surface is discussed. The effects of higher valence (W^{6+}) doping of TiO_2 carriers on H_2 and CO adsorption on Rh is discussed in the present communication, while the effects on kinetic parameters in CO hydrogenation and CO oxidation are discussed in a subsequent publication (9). The adsorption of H_2 on Rh (111) was investigated by Yates *et al.* (10), who observed a main TPD peak between 117 and 2°C, depending on surface coverage. A single desorption peak was also observed by Efstathiou and Bennett (11) over a 5.2% Rh/Al_2O_3 catalyst, while Bertucco and Bennett (12) detected two H_2 desorption peaks from a 10% Rh/SiO_2 catalyst. Apple *et al.* (13) detected three desorption peaks from Rh/TiO_2, following adsorption of H_2 at 300°C for 4 h and cooling to room temperature in H_2, all of which were attributed to H_2 desorption from Rh. In contrast, Stockwell *et al.* (14) attributed a high-temperature TPD peak to H_2 originating from the carrier, following a spillover process.

CO adsorbs molecularly on Group VIII metal surfaces (15, 16), in contrast to dissociative adsorption on other transition metal surfaces, and desorbs following first order kinetics (16). The TPD spectrum consists of a single peak (17, 18) with a shoulder on the low-T side of the major peak, which is attributed to CO adsorbed in the bridged mode. Significantly different TPD profiles are observed over Rh dispersed on high surface area carriers, in which case both CO and CO_2 are detected to desorb (19–21).

[1] To whom correspondence should be addressed.

0021-9517/94 $6.00

CO_2 is thought to originate from the Boudouard reaction and from the interaction of CO with hydroxyl groups of the carrier (20).

The aim of the present study is to investigate the influence of altervalent cation doping of the TiO_2 carrier on the interaction of H_2 and CO with supported Rh, in order to obtain relevant information concerning the chemisorptive and catalytic properties of this family of catalysts and also to obtain a better understanding of the interactions between the metal particles and the carrier.

EXPERIMENTAL

(a) *Support and Catalyst Preparation*

The parent titania carrier used in the present study was obtained from Degussa (P-25). X-ray diffraction analysis showed it to be 80% of the anatase form and 20% of the rutile form. To prepare the W^{6+}-doped TiO_2 carriers, weighed amounts of TiO_2 and WO_3 were slurried with distilled water and thoroughly mixed. The water was evaporated under continuous stirring and the residue was dried at 110°C for 24 h. The dried residue was then ground and sieved and was heat-treated in the presence of air as follows. The material was heated to 900°C with a heating rate of 4°C/min. It was maintained at 900°C for 5 h and then slowly cooled (approximately 10°C/min) to room temperature. During this heat treatment the doping cation diffuses into the crystal structure of TiO_2, which is entirely transformed to the rutile form, as shown by XRD analysis.

Catalysts were prepared by the method of incipient wetness impregnation of the support with appropriate amounts of aqueous solutions of $RhCl_3$ of concentration 5 mg $RhCl_3/cm^3$ and at a pH of approximately 2.5. Impregnated supports were dried at 110°C for 24 h. The dried material was then ground and sieved and placed in a stainless steel tube for reduction. The material was heated to 200°C with a heating rate of 5°C/min under nitrogen flow (50 cm^3/min). The flow was then switched to H_2 (50 cm^3/min) and the material was maintained at 200°C for 1 h; the temperature was then raised to 250°C with the same heating rate and was maintained at this temperature for 1 h under H_2 flow. The flow was then switched to N_2 and the catalyst was slowly cooled to room temperature and stored in air-tight vials until further use. The fact that the reduction temperature of 250°C is sufficient for complete reduction of Rh was experimentally verified by exposure of the catalysts to H_2 flow at higher temperatures (300 and 350°C). The adsorptive and catalytic properties of these catalysts were found to be identical to those reduced at 250°C.

The Rh content of the catalysts employed in the present study was invariably 0.5 wt%. The catalysts are designated as 0.5% Rh/TiO_2 (x% W^{6+}), where x is the dopant content in the carrier, in atom%.

(b) *Support and Catalyst Characterization*

The following techniques were employed in the characterization of supports and catalysts: (a) measurements of bulk electrical conductivity and activation energy of electron conduction of doped and undoped carriers, (b) selective equilibrium adsorption of H_2 and CO at room temperature, (c) transmission electron microscopy of selected samples.

Measurements of bulk electrical conductivity and activation energy of electron conduction of doped and undoped carriers were performed in the temperature range 100–300°C under a reducing (H_2) or inert (N_2) atmosphere. Details of the apparatus and the methodology employed for these measurements have been described in detail in a previous publication (5).

Adsorption isotherms of H_2 and CO were determined in a constant-volume high-vacuum apparatus (Micromeritics, Accusorb 2100E), in which an ultimate dynamic vacuum of 10^{-6} mm Hg could be obtained. Pressure detection was by means of a specially designed autoranging digital readout capacitance manometer with dual transducers. Adsorption isotherms of H_2 and CO were determined at 25°C, at equilibrium pressures between 10 and 300 mm Hg. Prior to adsorption measurements, the catalyst samples were evacuated at 200°C for 3 h, exposed to H_2 at 250°C for 1 h, and placed under dynamic vacuum for 8 h, during which period the sample was cooled to 25°C. Uptakes of H_2 and CO at monolayer coverage of the Rh particles, V_m, were obtained by extrapolation of the linear portions of the adsorption isotherms to zero pressure. Uptakes by unmetallized supports were found to be negligible, in all cases. The gases used were of ultrahigh purity and they were further purified by passing them through a Deoxo purifier and a molecular sieve trap.

For TEM analysis, the catalysts were ground to a fine powder and dispersed in methanol using an ultrasonic cleaner. A drop of the suspensions was placed onto a comvar-coated electron microscope grid. The average diameter of the Rh particles was estimated by measuring the diameter of over 200 particles from the microphotographs.

(c) *Temperature-Programmed Desorption Experiments*

The experimental setup for the TPD experiments has been described in detail in a previous publication (22). Prior to any experiments it was determined that the TPD cell and the tubing did not adsorb H_2 or CO and did not contribute to the mass spectrometer signal. The procedure for each experiment was the following. The catalyst, 0.5 g, was placed in the TPD cell, supported by quartz wool, and heated to 250°C in H_2 flow for 1 h. After purging with He for 15 min, the catalyst was cooled under He flow. When the desired adsorption temperature was reached, the He flow was switched to H_2 or CO flow. After 30 min

(H_2) or 15 min (CO), the flow was switched to He and the lines were cleaned for 3 min. Temperature programming was then initiated and the TPD profiles were obtained. At the end of each experiment with CO, the catalyst was exposed to O_2 at 450°C for 5 min to burn off possible carbon deposits. This procedure was found to give reproducible TPD results.

The design of TPD experiments and the selection of experimental parameters was done in such a way as to minimize mass transport and readsorption effects, as well as imperfect mixing in the TPD cell. The criteria proposed by Demmin and Gorte (23) were used for this purpose. The criteria concerning convective lag, diffusive lag, particle concentration gradients, and bed concentration gradients were found to be satisfied, indicating that the TPD cell operated as a CSTR without mass transport limitations. Readsorption effects may also influence TPD profiles. It has been shown that the elimination of readsorption effects in carrier gas TPD experiments over powdered catalysts requires experimental conditions which are not easily achievable (24, 25). It should be also stated that the low surface area and low porosity of the present catalysts tend to reduce readsorption effects.

RESULTS AND DISCUSSION

(a) *Measurements of Bulk Electrical Conductivity and Activation Energy of Electron Conduction*

Measurements of bulk electrical conductivity and activation energy of electron conduction were used to assess the influence of higher-valence cation doping on the electronic structure of the parent metal oxide, TiO_2. Titanium dioxide is a nonstoichiometric oxide with an excess of Ti^{n+} cations due to the presence of anionic vacancies or interstitial Ti^{n+} cations in the crystal matrix (26). Therefore, TiO_2 is an *n*-type semiconductor. Doping with higher-valence cations creates donor states and should increase its electrical conductivity (26). The measured electrical conductiviy, σ, of undoped and W^{6+}-doped TiO_2 under an atmosphere of H_2 is shown in Fig. 1 as a function of the inverse temperature. The dependence of electrical conductivity on temperature can be described by an Arrhenius type relationship of the form

$$\sigma = \sigma_0 \exp(-E_C/kT) \qquad (1)$$

where E_C is the activation energy of electronic conduction. It is apparent from Fig. 1 that doping of TiO_2 with W^{6+} cations increases the measured electrical conductivity by 2 to 3 orders of magnitude.

Electrical conductivity was also measured under an inert atmosphere (N_2) and was found to be significantly lower than that under H_2. This is an additional indication

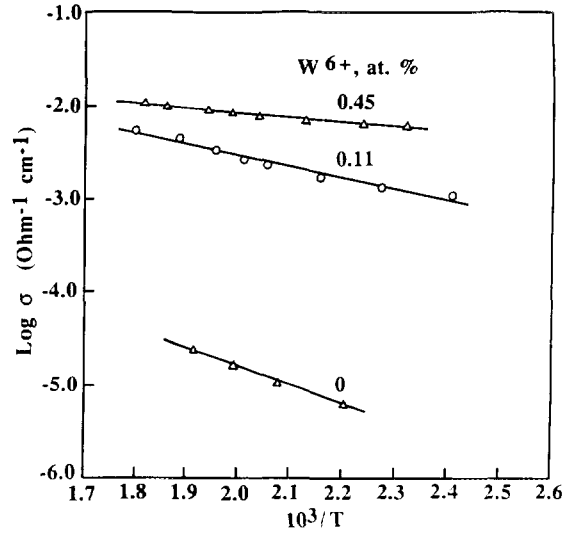

FIG. 1. Influence of W^{6+}-doping of TiO_2 on its electrical conductivity under a reducing (H_2) atmosphere in the temperature range 100–300°C.

of the *n*-type semiconducting character of TiO_2 (26). The enhancement of electrical conductivity under H_2 can be explained considering the following reactions of gaseous H_2 with the surface of the metal oxide,

$$H_2 + O_0 \leftrightharpoons H_2O\,(g) + V_0'' + 2e^- \qquad (2)$$

$$H_2 + 2O_0 \leftrightharpoons 2\,OH^- + 2e^-, \qquad (3)$$

where V_0'' represents the creation of an anionic vacancy and e^- represents a quasi-free electron.

In contrast, electrical conductivity is significantly reduced in the presence of O_2. For this reason, the resistance was beyond the capability of the instrument employed (>200 MΩ) and could not be measured. The reduction of electrical conductivity in the presence of O_2 can be explained by considering the reaction

$$O_2 + 2V_0'' + 4e^- \leftrightharpoons 2O_0 \qquad (4)$$

through which a large number of quasi-free electrons are consumed, resulting in reduced electrical conductivity.

The enhancement of electrical conductivity which is observed upon doping TiO_2 with cations of valence higher than that of the parent cation can be explained by considering the following defect-site reaction (5):

$$WO_3 \leftrightharpoons WO_2^{2+} + V_0'' + \tfrac{1}{2}O_2\,(g) + 2e^-. \qquad (5)$$

The absolute values of the electrical conductivity measurements are influenced by the effective contact between the grains pressed together to form the pellets (grain-boundary effects). In contrast, the activation energy of

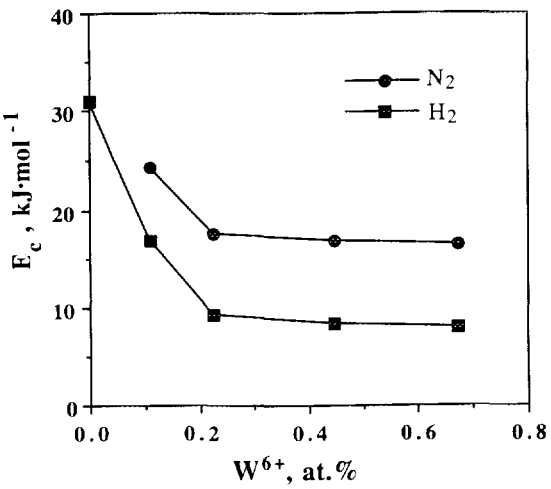

FIG. 2. Activation energy of electronic conduction of W^{6+}-doped TiO_2 under reducing (H_2) and inert (N_2) atmospheres.

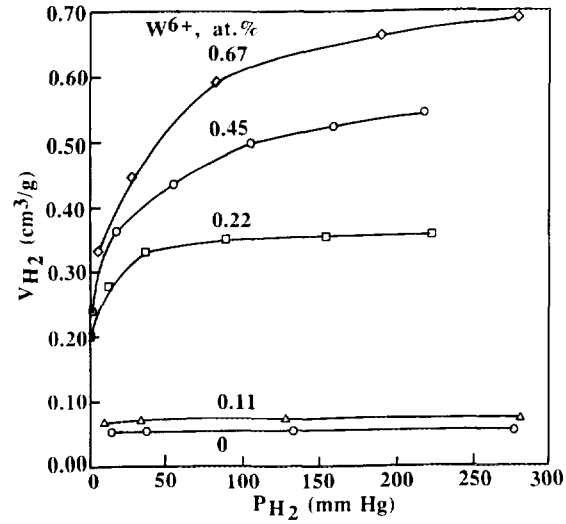

FIG. 3. Hydrogen adsorption isotherms on 0.5% Rh/TiO_2(x% W^{6+}) catalysts at 25°C.

electronic conduction is not affected by such phenomena (27) and, as a consequence, is a better indicator of alterations in the electronic structure of the semiconductor carrier, induced by higher-valence doping. The influence of W^{6+}-dopant concentration in the TiO_2 matrix on the activation energy of electronic conduction under an inert (N_2) or reducing (H_2) atmosphere is illustrated in Fig. 2. In both cases, the activation energy of electronic conduction is reduced significantly in the dopant concentration region between 0 and 0.22 at% (from ~30 to ~9 kJ/mol on doped TiO_2) and levels off at higher dopant concentration levels. The activation energy of electronic conduction is lower under a H_2 atmosphere for the reasons discussed earlier.

The values of activation energy obtained can be used to estimate the position of the donor energy level, E_d. The results presented above indicate that in the temperature range 100–300°C conductivity is defined by the electrons of the donor state. In this case, the activation energy of electronic conduction, E_c, is related to E_d by $E_C \approx E_d/2$ (28). Thus, E_d is 150–500 meV below the conduction band, depending on the gaseous atmosphere surrounding the semiconductor and the dopant content. The Fermi level in the temperature range 100–300°C should be close to the donor level. Based on these considerations, the work function of W^{6+}-doped TiO_2 should be in the neighborhood of 4.1–4.5 eV, significantly reduced as compared to that of undoped and unreduced TiO_2, which is 5.5 eV (29). This prediction is valid only as long as doping does not alter the electron affinity of TiO_2 or does not lead to the creation of a dipole layer on the TiO_2 surface.

(b) Influence of Altervalent Cation Doping on H_2 and CO Adsorption Capacity of Rh

The adsorption of H_2 and CO on 0.5% Rh/TiO_2(x% W^{6+}) catalysts was investigated at room temperature under equilibrium conditions. Preliminary adsorption experiments showed that the carriers were not active in either H_2 or CO adsorption under these conditions. Typical H_2 and CO adsorption isotherms are shown in Figs. 3 and 4, respectively. In most cases, the isotherms are well behaved and saturation coverage is attained at approximately 50–100 Torr in the case of H_2 and 30–50 Torr in the case of CO. It is apparent that the amount of H_2 adsorbed on the 0.5% Rh/TiO_2(x% W^{6+}) catalysts increases monotonically with increasing W^{6+}-dopant content in the carrier. This is not observed in the case of CO.

The amount of H_2 or CO adsorbed at monolayer coverage was obtained by extrapolation of the linear portions

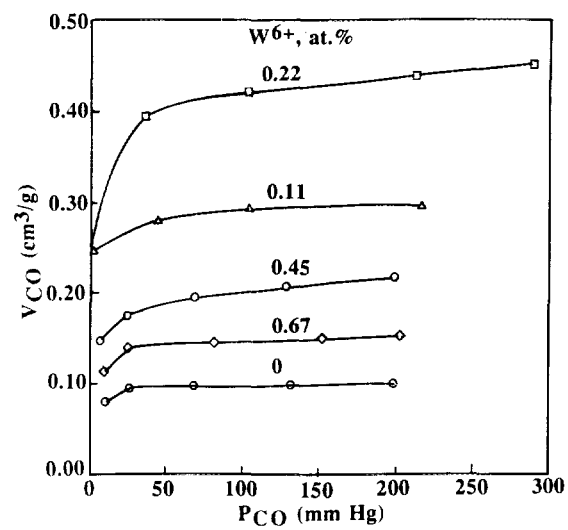

FIG. 4. Carbon monoxide adsorption isotherms on 0.5% Rh/TiO_2 (x% W^{6+}) catalysts at 25°C.

TABLE 1

H_2 and CO Adsorption Capacity of Rh Supported on Altervalent-Cation-Doped TiO_2

Support for 0.5% Rh	H/Rh	CO/Rh
TiO_2	0.10	0.09
TiO_2(0.11% W^{6+})	0.13	0.26
TiO_2(0.22% W^{6+})	0.62	0.37
TiO_2(0.45% W^{6+})	0.81	0.17
TiO_2(0.67% W^{6+})	0.99	0.13
TiO_2(0.66% Zn^{2+})	0.03	0.03
TiO_2(0.66% Mg^{2+})	0.02	0.02

TABLE 2

Average Rh Crystallite Size as Obtained by H_2 Adsorption and TEM

Support for 0.5% Rh	Average Crystallite Diameter (nm)	
	H_2 adsorption	TEM
TiO_2	11	8.2
TiO_2(0.22% W^{6+})	1.8	6.4

of the isotherms to zero pressure, which is a standard procedure. From these quantities, the H/Rh and CO/Rh ratios (number of H atoms or CO molecules adsorbed at monolayer coverage over the total number of metal atoms in the catalyst) are estimated and are presented in Table 1. The influence of the concentration of the W^{6+}-dopant in the TiO_2 matrix on the H_2 and CO adsorption capacity of the catalysts is illustrated in Fig. 5, in which the H/Rh ratio of the doped catalyst over the same ratio of the undoped catalyst, $[(H/Rh)_d/(H/Rh)_u]$, is shown as a function of the dopant content in the carrier. This ratio describes the degree of alteration of the adsorption capacity of the catalysts formulated on doped carriers. It is apparent that the H_2 adsorption capacity, at monolayer coverage, of W^{6+}-doped catalysts is significantly enhanced upon doping and it increases with increasing dopant content of the carrier. Thus, the 0.5% Rh/TiO_2 (0.67% W^{6+}) catalyst adsorbs approximately 10 times more hydrogen than the corresponding undoped catalyst. The CO adsorption capacity of the same catalysts is significantly different. The ratio $[(CO/Rh)_d/(CO/Rh)_u]$ increases drastically upon doping, goes through a maximum at approximately 0.22 at% W^{6+} in the carrier, and decreases at higher levels of doping, approaching values near unity at a W^{6+}-dopant content of 0.67 at%. The maximum enhancement of CO adsorption capacity, which is observed over the 0.5% Rh/TiO_2(0.22% W^{6+}) catalyst, is by approximately a factor of 4, as shown in Fig. 5.

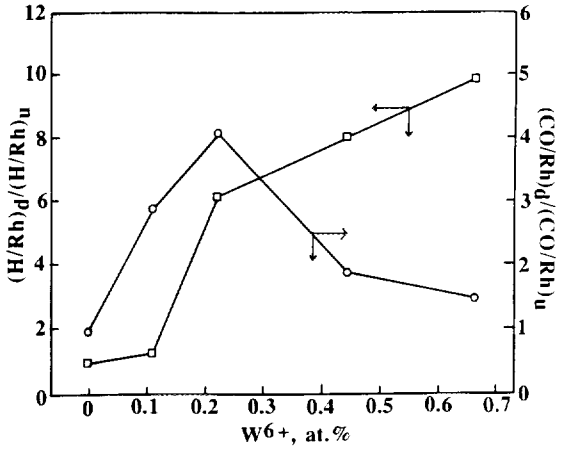

FIG. 5. Influence of W^{6+}-dopant content in the TiO_2 matrix on the H_2 and CO adsorption capacity of 0.5% Rh/TIO_2 (x% W^{6+}) catalysts at 25°C.

Rh catalysts dispersed on lower-valence doped TiO_2 (Zn^{2+}, Mg^{2+}) exhibited reduced H_2 and CO adsorption capacity at monolayer coverage. In the 0.5% Rh/TiO_2(0.66% Zn^{2+}) the H/Rh and CO/Rh ratios were found to be between 0.03 and 0.04, while in the 0.5% Rh/TiO_2(0.66% Mg^{2+}) catalyst they were approximately 0.02. The corresponding ratios $[(H/Rh)_d/(H/Rh)_u]$ and $[(CO/Rh)_d/(CO/Rh)_u]$ are then in the neighborhood of 0.3 to 0.7.

The influence of higher- or lower-valence doping of the TiO_2 carrier on the H_2 and CO adsorption capacity of Rh is the exact opposite of that observed with Pt (1). When Pt was dispersed over higher-valence (Ta^{5+}, Sb^{5+}, W^{6+})-doped TiO_2, its capacity to adsorb H_2 and CO was found to be reduced by approximately 80–90%. Lower-valence cation doping of TiO_2 was found not to influence significantly the capacity of Pt to adsorb H_2 or CO.

The alterations of the H_2 and CO adsorption capacity of Rh upon doping of the TiO_2 carrier with cations of higher or lower valence observed in the present study could be attributed to alterations in the degree of dispersion of the metal. To investigate this possibility, TEM analysis of the undoped as well as the 0.22 at% W^{6+}-doped catalysts was conducted, and the average crystallite size of each catalyst was estimated. Results are shown in Table 2. The average Rh crystallite size of the doped catalyst is somewhat lower (20%) than that of the undoped catalyst. This difference, however, cannot explain the enhanced H_2 adsorption, which for this catalyst is higher by a factor of 6. To illustrate this, the average particle diameter, as estimated from the H_2 adsorption results, is also included in Table 2. The value obtained for the doped catalyst is 1.8 nm, which is significantly smaller than the

value of 6.4 nm obtained from the TEM analysis. It can be concluded that the dispersion of Rh in the doped catalysts is not significantly different from that of the updoped catalysts. The same conclusion was reached in an earlier study concerning Pt dispersion on higher-valence doped TiO_2 carriers (1) by TEM analysis of the catalysts at all dopant concentration levels.

The fact that the observed alterations in adsorption capacity are not due to alterations in the degree of dispersion of Rh is also illustrated by comparison of the adsorption capacity of H_2 and CO, as shown in Fig. 5. If Rh supported on the doped carriers was of different dispersion, then the same trend would have been observed for H_2 and CO. However, at dopant levels higher than 0.22 at%, the H_2 adsorption capacity continues to increase with increasing dopant concentration, while the CO adsorption capacity decreases.

Another possible explanation for the enhancement of the H_2 adsorption capacity of W^{6+}-doped catalysts is hydrogen spillover from the metal to the carrier and subsequent reduction of WO_3. It has been reported in the literature (30, 31) that the reduction of WO_3 towards the bronze H_xWO_3, $x \sim 0.35$, can take place at room temperature in the presence of a Group VIII metal catalyst. The quantity of H_2 which could interact with WO_3 can be estimated, since the WO_3 content of the carriers is known. If it is assumed that the surface content of WO_3 is the same as that of the bulk (0.11–0.67 at%) and that the surface density of TiO_2 is $\sim 10^{19}$ atoms/m^2, then the surface density of W^{6+} cations is, at the maximum, 6×10^{16} W^{6+} cations/m^2. The quantity of H_2 required for bronze formation is approximately 3×10^{-3} cm^3H_2/g catalyst, which is negligible compared to the quantity of H_2 adsorbed on the catalysts (see Fig. 3). If it is assumed that the entire quantity of WO_3 is segregated to the surface of TiO_2 and that spilled-over hydrogen atoms can react with it, then the volume of H_2 required would be 0.17–1.0 cm^3/g catalyst, which is similar to the quantity of H_2 observed to adsorb at equilibrium. A number of arguments against this explanation can be offered: (a) ESCA analysis has failed to detect segregation of higher-valence dopants to the surface of TiO_2 (1); (b) the electrical conductivity measurements show that a major fraction of WO_3 is incorporated into the TiO_2 matrix, otherwise no significant alterations in conductivity would have been observed; (c) the same phenomenon should have been observed with Pt, whereas, as stated earlier, the amount of H_2 adsorbed on Pt/TiO_2 ($x\%$ W^{6+}) catalysts was found to be dramatically lower than that of undoped catalysts (1); (d) the shapes of the adsorption isotherms would have been distorted, if such a process was taking place we recall that the adsorption at monolayer coverage was obtained by extrapolation of the isotherms to zero pressure, and (e) such an explanation can account neither for the CO adsorption behavior nor for the increased CO adsorption capacity.

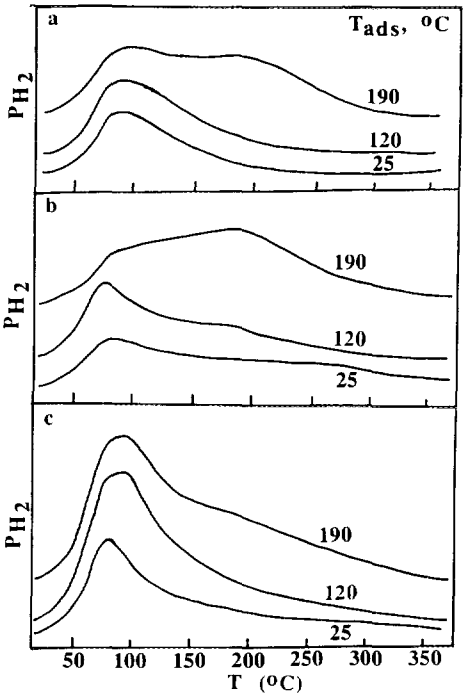

FIG. 6. TPD profiles of H_2 following adsorption at 25, 120, and 190°C from (a) 0.5% Rh/TiO_2(0% W^{6+}), (b) 0.5% Rh/TiO_2(0.11% W^{6+}), and (c) 0.5% Rh/TiO_2(0.45% W^{6+}) catalysts.

From the discussion above it can be concluded that the abnormal H_2 and CO adsorption behavior of Rh dispersed on TiO_2 carriers doped with higher valence (W^{6+}) or lower valence (Zn^{2+}, Mg^{2+}) cations is due to an interaction between the Rh crystallites and the doped semiconductor carrier. This interaction has been described in the past (1–4, 6–8) as an electronic one, which may alter the work function of surface metal atoms. This theory will be further elaborated on in a subsequent section.

(c) *Temperature-Programmed Desorption of H_2*

TPD profiles of H_2 from the 0.5% Rh/TiO_2 ($x\%$ W^{6+}) catalysts were obtained following H_2 adsorption at 25, 120, and 190°C. No H_2 was detected to desorb from unmetallized carriers. The TPD profiles obtained from the undoped catalyst are shown in Fig. 6a. At low adsorption temperatures (25 and 120°C) a single desorption peak is apparent with maximum at approximately 90°C. A second desorption peak appears at approximately 190°C, when H_2 adsorption takes place at 190°C. The corresponding profiles from the 0.5% Rh/TiO_2 (0.11% W^{6+}) and 0.5% Rh/TiO_2(0.45% W^{6+}) catalysts are shown in Figs. 6b and 6c, respectively. The profiles from the 0.5% Rh/TiO_2 (0.11% W^{6+}) catalyst are quite similar to those of the

TABLE 3

Hydrogen Desorption Peak Temperatures (T_M) Observed for 0.5% Rh/TiO_2 (x% W^{6+}) Catalysts Following Adsorption at Different Temperatures (T_{ads})

x at%	Desorption Peak Temperature T_M (°C)		
	T_{ads} = 25°C	T_{ads} = 120°C	T_{ads} = 190°C
0	84	88	93, 190
0.11	77	77	83, 190
0.22	98	—	113
0.45	77	88	93, 170
0.67	95	100	103, 195

undoped catalyst. At low adsorption temperature, a single desorption peak is observed at 75–77°C, while, at high adsorption temperature, a second desorption peak at 190°C appears. The profiles from the 0.5% Rh/TiO_2(0.45% W^{6+}) catalyst consist of a single peak, which is shifted from 77 to approximately 90°C, as the adsorption temperature is raised from 25 to 190°C. The second desorption peak, when adsorption takes place at 190°C, is not clearly resolved, appearing as a broad shoulder to the main peak.

Desorption peak temperatures of all catalysts following H_2 adsorption at different temperatures are summarized in Table 3. Peak temperatures do not show any specific trend with variation of W^{6+}-dopant content in the carrier, being in the range of 77 to 98°C, for an adsorption temperature of 25°C. Nevertheless, a trend towards higher desorption temperatures with increasing adsorption temperature is observed. This trend cannot be explained by assuming that the surface coverage increases at higher adsorption temperatures since, in that case, the opposite trend would be expected, as predicted for second order desorption with or without readsorption phenomena (25). Therefore, this shift must be attributed to stronger Rh–H bonds, which are formed at higher adsorption temperatures. It is also apparent in Table 3 that the second desorption peak appears only when adsorption takes place at elevated temperatures. This peak corresponds to strongly adsorbed hydrogen, the adsorption of which might be an activated process.

The quantity of H_2 detected to desorb from the 0.5% Rh/TiO_2 (x% W^{6+}) family of catalysts is shown in Table 4. The quantity of H_2 observed to adsorb at equilibrium at 25°C is also reported in Table 4 for comparison purposes. In all cases the quantity of desorbed H_2 increases with increasing adsorption temperature, which might imply that H_2 adsorption on these catalysts is partly an activated process. Activated H_2 adsorption on Rh/TiO_2 catalysts, but not on Rh/Al_2O_3 and Rh/SiO_2, has been reported in a previous publication (22), in which it was also demonstrated that surface contamination is not a probable cause of the enhancement of H_2 adsorption on Rh/TiO_2 catalysts at elevated temperatures. The quantity of H_2 desorbed following adsorption at 25°C is smaller than that adsorbed in the static equilibrium experiments. This is due to either of the following reasons. (a) The static adsorption measurements correspond to equilibrium conditions and have been obtained following a time of adsorption in excess of 10 h. In contrast, in the TPD experiments adsorption takes place under H_2 flow for 30 min, time which might not be sufficient to reach equilibrium. (b) A fraction of adsorbed H_2 could be desorbing prior to initiation of the TPD experiment, while the sample is exposed to He flow for 3–5 min, so as to clean the lines and stabilize the mass spectrometer signal (32).

In a final set of experiments it was investigated to what extent CO could displace H_2 from the surface of the 0.5% Rh/TiO_2(x% W^{6+}) family of catalysts. After H_2 was adsorbed at 190°C for 30 min and the sample was cooled to room temperature under H_2 flow, the flow was switched to He for 5 min to remove H_2 from the gas phase, and then the sample was exposed to CO flow for 5 min. The TPD profile of H_2 was obtained following this treatment. In the case of the undoped catalyst, no H_2 desorption under 250°C was observed, indicating that nearly the entire quantity of adsorbed H_2 had been displaced by CO. Profiles obtained from the other catalysts are shown in Fig. 7. In the 0.5% Rh/TiO_2(0.11% W^{6+}) catalyst, CO has displaced the weakly adsorbed H_2 but the strongly adsorbed H_2 has remained, giving a peak at approximately 200°C. For the catalyst with higher levels of doping, the main H_2 peak, at approximately 100°C is maintained, indicating that the ability of CO to displace H_2 from the surface is gradually reduced, as the W^{6+} dopant concentration in the carrier increases. This could be attributed to either strengthening of the Rh–H bond, which, however, was not observed in the experiments discussed previously, or to weakening of the interaction between Rh and CO, which is further analyzed below. It should be noted that in

TABLE 4

Quantity of Hydrogen Detected to Desorb from the 0.5% Rh/TiO_2 (x% W^{6+}) Catalysts and Quantity of H_2 Adsorbed at Equilibrium at 25°C

x at%	H_2 desorbed (cm^3/g) for T_{ads} (°C)			H_2 adsorbed at equilibrium (25°C) (cm^3/g)
	25	120	190	
0	0.03	0.05	0.06	0.05
0.11	0.11	0.13	0.23	0.07
0.22	0.15	—	0.29	0.34
0.45	0.19	0.33	0.38	0.44
0.67	0.20	0.45	0.55	0.54

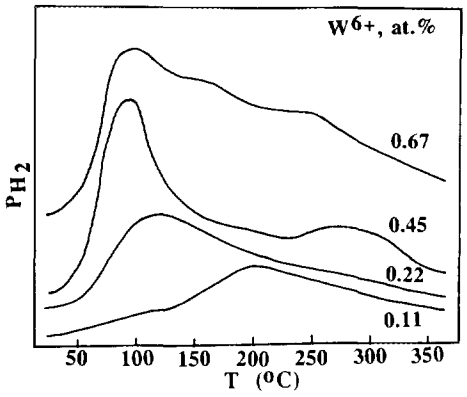

FIG. 7. TPD profiles of H_2 following H_2 adsorption at 190°C, cooling to 25°C in H_2 flow, and exposure to CO for 5 min at the same temperature.

the profiles of Fig. 7, H_2 which is detected at temperatures higher than approximately 250°C, does not correspond to H_2 desorbing from Rh, but to H_2 produced by interaction of CO with the surface of the carrier as discussed below.

(d) Temperature-Programmed Desorption of CO

TPD profiles of CO were obtained following adsorption on the 0.5% Rh/TiO_2 (x% W^{6+}) family of catalysts at room temperature, in the continuous flow mode for 15 min. The unmetallized carriers were found not to adsorb detectable quantities of CO. During the TPD experiments, the following mass numbers were continuously monitored in the mass spectrometer: 28 (CO), 44 (CO_2), 2 (H_2), and 15 (CH_4).

TPD profiles after CO adsorption on the undoped catalyst are shown in Fig. 8a. The CO profile consists of two main peaks at approximately 119 and 202°C, while a smaller peak is apparent at approximately 380°C. The CO_2 profile consists of a single broad peak at approximately 300°C. The CO_2 evolution is accompanied by H_2 evolution. The CO_2 and H_2 profiles are similar, which indicates that they might have a common origin which could be the reaction (11, 20)

$$CO_{(a)} + H_2O_{(g)} \rightarrow CO_2 + H_2 \qquad (6)$$

or the reaction

$$CO + OH_{(s)} \rightarrow (HCOO)_{(a)} \rightarrow CO_2 + \tfrac{1}{2}H_2. \qquad (7)$$

The first reaction takes place between adsorbed CO and H_2O, which either is found as an impurity in the carrier gas, or is adsorbed on the catalyst surface, and leads to equal quantities of CO_2 and H_2 produced. The second reaction describes the interaction between CO and surface hydroxyls of the carrier, with CO_2 and H_2 as final products with a 2 to 1 ratio. The evolved quantity of H_2 was found to be approximately half of that of CO_2 indicating that the second reaction is more probable. Furthermore, as indicated earlier, particular attention was paid to purifying the gases used in the TPD experiments so as to minimize parasitic reactions such as that between CO and H_2O. Therefore, the role of the metal in this process is to retain CO on the catalyst surface up to fairly high temperatures, where it is more likely to react with hydroxyl groups as it desorbs and diffuses through the catalyst bed. On the basis of this reasoning it can be concluded that the position of the CO_2 peak in the temperature scale reflects the strength of the adsorption of CO from which it originates. The possibility that part of desorbed CO_2 originates from dissociation of CO (Boudouard reaction) cannot be excluded. However, as is shown in a subsequent publication (9), CO dissociation is decreased on doped catalysts.

Corresponding TPD profiles obtained over the 0.5% Rh/TiO_2(0.22% W^{6+}) and 0.5% Rh/TiO_2(0.45% W^{6+}) are shown in Figs. 8b and c, respectively. H_2 profiles, which are not shown, were similar to the CO_2 profiles. CH_4 was also observed to desorb in very small quantities, generally

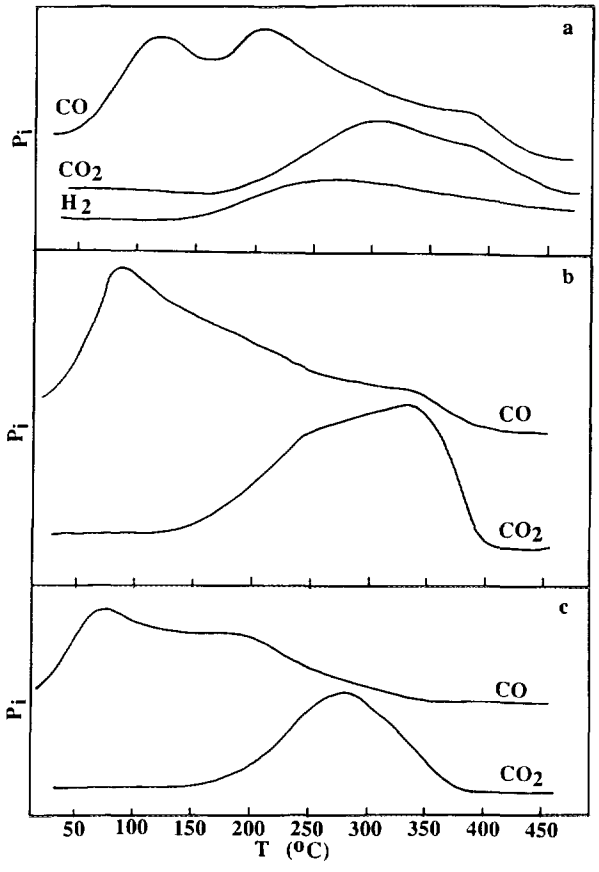

FIG. 8. TPD profiles of CO, CO_2, and H_2 following CO adsorption at 25°C over (a) 0.5% Rh/TiO_2(0% W^{6+}), (b) 0.5% Rh/TiO_2(0.22% W^{6+}), and (c) 0.5% Rh/TiO_2(0.45% W^{6+}) catalysts.

TABLE 5

Peak Temperatures of TPD Profiles from the 0.5% Rh/TiO_2 (x% W^{6+}) Family of Catalysts Following CO Adsorption at 25°C

x at%	T_M (°C)	
	CO	CO_2
0	119, 202, 380	300, 380
0.11	104, —, 360	240, 360
0.22	85, —, 330	250, 330
0.45	70, 180, —	278
0.67	77, 160, —	270

less than 1% of the total quantity of desorbed gases. The CO profile from the 0.5% Rh/TiO_2 (0.22% W^{6+}) catalyst consists of a single main peak at approximately 85°C with a shoulder on the high-T side. A second, much smaller peak is also observed at approximately 330°C. The CO_2 profile consists of a broad peak covering the range of 150 to 380°C. The CO profile from the 0.5% Rh/TiO_2(0.45% W^{6+}) catalyst consists of a major peak at approximately 70°C and a smaller one at 180°C. The CO_2 profile consists of a broad peak with a maximum at approximately 278°C.

Peak temperatures observed during CO TPD over the entire family of catalysts are summarized in Table 5. It is apparent that the CO peaks are shifted towards lower temperatures as the W^{6+} content in the carrier increases. The main CO peak is shifted from 119°C for the undoped catalyst to 70–77°C for the catalysts containing 0.45–0.67 at% W^{6+}. The peak at 202°C for the updoped catalyst is not apparent in the case of 0.11 and 0.22 at% W^{6+} catalysts, but it appears again, at lower temperatures (160–180°C) when the dopant concentration is further increased. The small peak at 380°C is also shifted towards lower temperatures and disappears at high levels of doping. The broad CO_2 peak seems to consist of two overlapping peaks at 300 and 380°C in the undoped catalyst which shift to 240, 360°C and 250, 330°C at low levels of W^{6+} doping. At higher levels of doping the two peaks seem to merge into a single one at 270–278°C.

These observations indicate that the adsorption of CO on Rh supported on higher-valence doped TiO_2 is weakened and that the degree of alteration of the strength of the Rh–CO adsorption bond is a function of the concentration of the dopant in the TiO_2 matrix. This is in contrast to the results obtained from the H_2 TPD experiments. In that case, an increase in the quantity of H_2 desorbed with increasing dopant content was observed. However, no significant shifts in peak temperatures with dopant content were observed. It was also found that in the doped catalysts, preadsorbed H_2 could not be easily displaced by CO, as was the case for the undoped catalyst. This observation can now be explained taking into consideration the fact that the interaction between CO and Rh in the doped catalysts is weakened, which reduces the competitive advantage of CO for adsorption on the metal surface.

(e) *Interpretation*

The effects of altervalent cation doping of TiO_2 on the chemisorptive and catalytic properties of supported Pt crystallites have been discussed in previous publications (1–4) in the framework of the metal–semiconductor boundary layer theory. Solymosi and co-workers (7, 8) have also applied this theory to the interpretation of the interaction between TiO_2 and supported Ni or Rh. Detailed descriptions of this theory can be found in the literature (28, 33, 34). Briefly, this theory predicts that if a metal is in contact with a semiconductor, the two solids possess the same electrochemical potential at thermodynamic equilibrium. This implies that if initially (before contact), the metal and the semiconductor have different electrochemical potentials, then upon contact, transfer of electrons will take place towards the material with the lower electrochemical potential until the two potentials are equalized.

The experimental observations made in the present study, involving Rh crystallites, are similar (although frequently in the opposite direction) to those made over Pt. Based on the theory and the findings discussed above, the Rh–TiO_2 system, in most probability, forms a Schottky barrier junction, since the work function of Rh (~5 eV) (35) is higher than that of reduced TiO_2 (4.6 eV) (29). When TiO_2 is doped with cations of higher valence (W^{6+}), its work function is further reduced, as shown by the measurements of electrical conductivity and activation energy of electron conduction which were discussed earlier. Therefore, electrons are transferred from the doped semiconductor carrier to the Rh crystallites. The quantity of charge transferred depends on the concentration of the dopant in the carrier and the gaseous atmosphere under which the catalyst exists. For example, the contact between Pd or Pt and TiO_2 is of the Schottky type under air, but becomes ohmic in the presence of hydrogen (36–38). This is due to the fact that species adsorbed on the surface of the metal or the semiconductor influence their work function in either the positive or negative direction, depending on the donor or acceptor character of the adsorbate.

The electrons which are transferred to the metal occupy empty energy states at the Fermi level. This can lead to a rise of the Fermi level and a reduction of the chemical potential of the metal (39), as shown schematically in Fig. 9. The reduction of the chemical potential is expected to be negligible for large metal particles, since transition metals have a large density of states. In small metal parti-

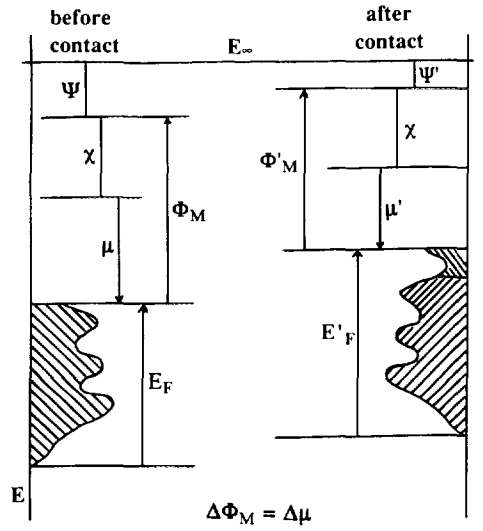

FIG. 9. Influence of charge transfer to the metal–semiconductor boundary layer on the electronic structure of the metal particles.

cles, however, such as those found in supported metal catalysts (1–10 nm), the alteration of the chemical potential could be significant. In contrast, the surface potential of the free metallic surface is not expected to be influenced, since the charge which is transferred is located on the interface metal atoms (40). Therefore, the reduction of the chemical potential corresponds to an equal reduction of the work function of the metal particles, as shown in Fig. 9. In this way, the electronic interaction at the metal–semiconductor interface influences the electron structure (work function) of the surface metal atoms and thus is referred to as long-range interaction.

In addition to the long-range interaction, the potential of localized or short-range interactions must also be considered. The atoms at the periphery of the metal particles possess a high concentration of negative charge, while, in the same region, strong electrostatic fields are present due to the existence of the dipole at the interface. It has been estimated (40) that the intensity of the electric field in this region is of the order of 10^6–10^7 V/cm, depending on the size of the metal particles. Vanselow and Mundschau (41) report that such electric fields could influence significantly the rates of surface reactions. The effect of strong electric fields on NO adsorption on Pt(111) and Rh(111) has been studied theoretically and experimentally (42–44). It was observed that the adsorption of NO on Rh(111) is influenced by high electric fields and that the electric field acts in a manner similar to work function changes or alkali coadsorption. More specifically, it was found that a field strength of 3 V/nm decreases by approximately 15% the binding energy of NO on Rh(111). It should be noted that the adsorption characteristics of CO are similar to those of NO. In small metal particles the number of atoms at the three-phase boundary (metal–semiconductor–gas) can be a significant fraction of the exposed metal atoms. In that case, alterations in chemisorptive and catalytic parameters could be primarily due to this short range or localized interaction. Both long-range and short-range effects are quantified, to the extent possible, in a subsequent publication (40).

A question of interest with respect to the theory discussed above, is whether small metal particles such as those found in supported metal catalysts (1–10 nm) preserve their metallic properties. When the number of atoms in a metal particle is small, the electron energy states cannot be considered as a continuous band. The distance Δ between two energy states is proportional to E_F/N, where E_F is the Fermi energy and N the number of atoms in the particle (45). It has been proposed that quantum size effects will be significant when $\Delta > kT$ (45). Temperatures of interest in catalysis are generally higher than 300 K, in which case the value of kT is approximately 0.026 eV. Considering a typical value of E_F of around 7 eV (39, 46), a critical number of atoms in a metal particle, N_{min}, is approximately 250 atoms. In the case of Rh this corresponds to a spherical particle of radius of 9 Å. A similar size is also predicted for the case of Pt. Thus, it can be concluded that metal particles larger than approximately 2 nm may be expected to possess typical metallic properties. In contrast, in smaller particles the metallic character is gradually reduced and this can significantly influence their chemisorptive and kinetic properties.

The results of H_2 and CO adsorption of Rh crystallites dispersed on TiO_2 doped with higher valence cations can be discussed with respect to the long and short range effects on the electronic structure of the Rh particles, caused by doping of the semiconducting carrier. The equilibrium adsorption of H_2 was found to be enhanced upon W^{6+}-doping and the enhancement was found to increase with dopant concentration in the carrier. The TPD experiments showed that the strength of the Rh-H adsorption bond is not altered upon doping. It has been shown (47) that hydrogen adsorption on metals has a homopolar character and the work function of the metal is not significantly altered upon adsorption. Therefore, it can be concluded that the strength of the adsorption bond is not affected, to a great extent, by the work function of the metallic surface, which is consistent with the results of the present study. The enhancement of the quantity of H_2 adsorbed can be attributed to a change in the stoichiometry of hydrogen adsorption due to enhancement of the electron density of states or to the creation of new adsorption sites at the periphery of the metal–support interface. Because of the electron transfer to the Rh crystallite, the support region (depletion region) around the Rh particle is positively charged and strong electrostatic fields are created at the metal–support interface (40). The creation of new

adsorption sites can be ascribed to these two factors. Since the alteration of the adsorption capacity is significant, the creation of new adsorption sites, referring to both metal and carrier atoms at the periphery of the interface, is a more probable mechanism than a change in the stoichiometry of hydrogen adsorption on Rh.

Concerning CO adsorption, the TPD experiments have shown weakening of the Rh–CO bond when Rh is dispersed on W^{6+}-doped TiO_2 carriers, which is not accompanied by reduction of the quantity of strongly adsorbed CO. CO chemisorption on Rh takes place through the formation of a σ-bond between the 5σ CO orbital and empty *d*-orbitals of Rh (electron transfer from CO to Rh) and a π-bond between the filled *d*-orbitals of Rh and the empty π^*-orbital of CO (back-donation, electron transfer from Rh to CO) (48, 49). The net charge transfer is from the metal to the CO molecule. Enhancement of the electron density and reduction of the work function of surface Rh atoms, as might be the case for Rh supported on W^{6+}-doped TiO_2, is expected to inhibit the formation of the σ-bond and to increase back-donation from Rh to CO, thereby strengthening the Rh–C bond and weakening the C–O bond. This mechanism has been used to explain the increase in the heat of adsorption and the dissociation probability of CO in the presence of electropositive impurities (e.g. K) on the metal surface, which also lead to a reduction of the surface work function (50–53). One would expect a similar increase in the Rh–CO bond strength on doped catalysts. TPD experiments, however, indicated that the Rh–CO bond is weaker on doped catalysts and, as is shown in a subsequent publication (9), CO dissociation is also suppressed, which is in harmony with the TPD results. It can be speculated that this is due to hybridization of the Rh orbitals because of the electron transfer (54) and this new configuration interacts less strongly with the CO molecule. Short-range effects can also play a role. It was discussed earlier that strong electric fields lead to a decrease of NO binding energy on Rh(111) (42–44). The presence of strong electrostatic fields at the Rh-doped TiO_2 interface (40) can have an analogous effect on CO binding energy.

CONCLUSIONS

The following conclusions can be drawn from the results of the present study.

1. The electronic structure of TiO_2 is significantly altered upon doping with higher valence cations (W^{6+}). In particular, electrical conductivity is increased by 2–3 orders of magnitude and the activation energy of electronic conduction is reduced.

2. Supported Rh catalysts formulated on W^{6+}-doped TiO_2 carriers exhibit an enhanced capacity for H_2 adsorption, which increases with dopant concentration. The capacity of these catalysts to adsorb CO is also enhanced and it exhibits a maximum with increasing dopant concentration.

3. H_2 TPD from W^{6+}-doped catalysts revealed that the strength of the Rh–H bond is not significantly altered with doping. In contrast, the Rh–CO adsorption bond strength is weakened when Rh is dispersed on W^{6+}-doped TiO_2.

4. Alterations in the chemisorptive properties of the Rh crystallites dispersed on W^{6+}-doped TiO_2 carriers are attributed to long-range or short-range electronic interactions at the metal–carrier interface which alter the electronic structure of surface and interface metal atoms.

REFERENCES

1. Akubuiro, E. C., and Verykios, X. E., *J. Catal.* **103,** 320 (1987).
2. Akubuiro, E. C., and Verykios, X. E., *J. Catal.* **113,** 106 (1988).
3. Akubuiro, E. C., Ioannides, T., and Verykios, X. E., *Appl. Catal.* **46,** 297 (1988).
4. Akubuiro, E. C., Verykios, X. E., and Ioannides, T., *J. Catal.* **116,** 590 (1989).
5. Akubuiro, E. C., and Verykios, X. E., *J. Phys. Chem. Solids* **50,** 17 (1989).
6. Schwab, G. M., *in* "Advances in Catalysis" (D. D. Eley, H. Pines, and P. B. Weisz, Eds.), Vol. 27, p. 1. Academic Press, New York, New York, 1978.
7. Solymosi, F., *Catal. Rev.* **1,** 233 (1967).
8. Solymosi, F., Tombacz, I., and Koszta, J., *J. Catal.* **95,** 578 (1985).
9. Ioannides, T., Verykios, X. E., Tsapatsis, M., and Economou, C., *J. Catal.* **145,** 491 (1994).
10. Yates, J. T., Thiel, P. A., and Weinberg, W. H., *Surf. Sci.* **84,** 427 (1979).
11. Efstathiou, A. M., and Bennett, C. O., *J. Catal.* **124,** 116 (1990).
12. Bertucco, A., and Bennett, C. O., *Appl. Catal.* **35,** 329 (1987).
13. Apple, T. M., Gajardo, P., and Dybowski, C., *J. Catal.* **68,** 103 (1981).
14. Stockwell, D. M., Bertucco, A., Coulson, G. W., and Bennett, C. O., *J. Catal.* **113,** 317 (1988).
15. Yates, J. T., Williams, E. D., and Weinberg, W. H., *Surf. Sci.* **91,** 562 (1980).
16. Thiel, P. A., Williams, E. D., Yates, J. T., and Weinberg, W. H., *Surf. Sci.* **84,** 54 (1979).
17. Mate, C. M., and Somorjai, G. A., *Surf. Sci.* **160,** 542 (1985).
18. Bertel, E., Rosina, G., and Netzer, F. R., *Surf. Sci.* **172,** L515 (1986).
19. Erdöhelyi, A., and Solymosi, F., *J. Catal.* **84,** 446 (1983).
20. Efstathiou, A. M., Ph. D. Dissertation. University of Connecticut, 1989.
21. Oh, S. H., and Eickel, C. C., *J. Catal.* **112,** 543 (1988).
22. Ioannides, T., and Verykios, X., *J. Catal.* **140,** 353 (1993).
23. Demmin, R. A., and Gorte, R. J., *J. Catal.* **90,** 32 (1984).
24. Rieck, J.S., and Bell, A. T., *J. Catal.* **85,** 143 (1984).
25. Ioannides, T., and Verykios, X. E., *J. Catal.* **120,** 157 (1989).
26. Solymosi, F., *in* "Contact Catalysis" (Z. G. Szabó and D. Kalló, Eds.), Vol. 1. Elsevier, Amsterdam, 1976.
27. Herrmann, J. M., and Pichat, P., *J. Catal.* **78,** 425 (1982).
28. Sze, S. M., "Physics of Semiconductor Devices," 2nd ed. Wiley, New York, 1985.
29. Chung, Y. W., Lo, W. J., and Somorjai, G. A., *Surf. Sci.* **64,** 588 (1977).
30. Boudart, M., and Djega-Mariadassou, G., "Kinetics of Heterogeneous Catalytic Reactions." Princeton Univ. Press, Princeton, NJ, 1984.

31. Sermon, P. A., and Bond, G. C., *Catal. Rev.* **8,** 211 (1973).
32. Jones, R. D., and Bartholomew, C. H., *Appl. Catal.* **39,** 77 (1988).
33. Tyagi, M. S., in "Metal–Semiconductor Schottky Barrier Junctions and Their Applications" (B. L. Sharma, Ed.). Plenum, New York, 1984.
34. Brillson, L. J., *Surf. Sci. Rep.* **2,** 123 (1982).
35. Dean, J. A., "Lange's Handbook of Chemistry," 14th ed. McGraw–Hill, New York, 1992
36. Yamamoto, N., Tonomura, S., Matsuoka, T., and Tsubomura, H., *Surf. Sci.* **92,** 400 (1980).
37. Yamamoto, N., Tonomura, S., Matsuoka, T., and Tsubomura, H., *J. Appl. Phys.* **52,** 6227 (1981).
38. Yamamoto, N., Tonomura, S., and Tsubomura, H., *J. Electrochem. Soc.* **129,** 444 (1982).
39. Ashcroft, N. W., and Merwin, N. D., "Solid State Physics." Holt, Rinehart & Winston, New York, 1976.
40. Ioannides, T., and Verykios, X. E., submitted for publication.
41. Vanselow, R., and Mundschau, M., *J. Catal.* **103,** 426 (1987).
42. Kreuzer, H. J., and Wang, L. C., *J. Chem. Phys.* **93,** 6065 (1990).
43. Block, J. H., Kreuzer, H. J., and Wang, L. C., *Surf. Sci.* **246,** 125 (1991).
44. Madenach, R. P., Abend, G., Mousa, M., Kreuzer, H. J., and Block, J. H., *Surf. Sci.* **266,** 56 (1992).
45. Harrison, M. R., and Edwards, P. P., *in* "The Metallic and Nonmetallic States of Matter" (Edwards, P. P., and Rao, C. N. R., Eds.). Taylor & Francis, London, 1985.
46. Moruzzi, V. L., Janak, J. F., and Williams, A. R., "Calculated Electronic Properties of Metals." Pergamon, New York, 1978.
47. Shimizu, H., Christmann, K., and Ertl, G., *J. Catal.* **61,** 412 (1980).
48. Kiskinova, M., *in* "New Trends in CO Activation" (L. Guczi, Ed.), Studies in Surface Science and Catalysis, Vol. 64, p. 37. Elsevier, Amsterdam, 1991.
49. Ponec, V., *in* "New Trends in CO Activation" (L. Guczi, Ed.), Studies in Surface Science and Catalysis, Vol. 64, p. 117. Elsevier, Amsterdam, 1991.
50. Luftman, H. S., Sun, Y. M., and White, J. M., *Appl. Surf. Sci.* **19,** 59 (1984).
51. Crowell, J. E., and Somorjai, G. A., *Appl. Surf. Sci.* **19,** 73 (1984).
52. Bertolini, J. C., Delichère, P., and Massardier, J., *Surf. Sci.* **160,** 531 (1985).
53. Weimer, J. J., Umbach, E., and Menzel, D., *Surf. Sci.* **155,** 132 (1985).
54. Chen, H.-W., White, J. M., and Ekerdt, J. G., *J. Catal.* **99,** 293 (1986).